ACES Asian Chemical Editorial Society

DOI: 10.1002/cnma.201600105

CHEMNANOMAT
Communication

Aerogels

Free-Standing Graphene-Encapsulated Silicon Nanoparticle Aerogel as an Anode for Lithium Ion Batteries

Xiaozhen Hu, Yan Jin, Bin Zhu, Yingling Tan, Su Zhang, Linqi Zong, Zhenda Lu, and Jia Zhu*[a]

Abstract: Silicon is a remarkable candidate for lithium-ion battery anodes, due to the highest theoretical specific capacity, low working potential, and abundance on earth. However, the volume of Si changes ≈300% during the lithiation–delithiation cycling, leading to pulverization and poor electrical contact between Si and the current collector, resulting in fast fading capacity. To overcome these problems, we develop a novel free-standing anode by encapsulating Si nanoparticles into a lightweight, flexible, and conductive graphene network by utilizing a facile freeze-drying strategy. The Si nanoparticles are tightly anchored on the ultrathin and flexible graphene sheets, which can serve as mechanical support, electrical network, and buffer layer for Si. This free-standing aerogel exhibits superior electrochemical performance, and the specific capacity is 617 mA h g^{-1} after 50 cycles at a current density of 0.8 A g^{-1}, 4 times that of a traditional Si electrode on Cu foil fabricated by a typical slurry method.

Rechargeable lithium-ion batteries (LIBs) play a dominant role in daily life due to their high energy and power density. To meet the ever-growing demands of energy storage, the development of LIBs with higher energy capacity and longer cycle life is of great importance.[1] Among all the candidates for anode materials, Si exhibits the highest theoretical capacity (4200 mA h g^{-1}, $Li_{22}Si_5$), ≈11 times of that of a commercial graphite anode (372 mA h g^{-1}), and a low discharge potential (370 mV vs. Li/Li$^+$). In addition, it is the second most abundant element on earth.[2,3] Thus Si has been regarded as one of the most promising anode materials for next-generation LIBs. Unfortunately, there is a well-known issue for Si as an anode, the fast fading of capacity during the charge–discharge cycling due to the 300% volume change, which leads to particle fracture, loss of electrical contact, and unstable solid-electrolyte interphase (SEI).[4,5]

Various approaches have been carried out to address these issues.[6–15] One typical strategy is to design various nanostructures to withstand the large (de)lithiation strains, including Si nanowires,[6] nanotubes,[7] porous Si,[8,9] hollow particles,[10] and so on.[11,12] Another way is coating a stable protecting layer on Si to prevent electrolyte infiltration and provide interior void space for volume expansion, such as Si–SiO_2 hollow tubes,[13] the Si–C yolk–shell,[14] and pomegranate structures.[15] These two existing processes show great potential to overcome the pulverization, poor electrical contact, and unstable SEI problems. However, most of the electrode preparation relies on coating films of active materials, conductive additives, and polymer binders on metal foils, which are much heavier than Si active material, bringing low energy density. In addition, the polymer binders could block ion transport and degrade the electrical conductivity of anode, inducing rapid loss of capacity.[16] Therefore, it is important to investigate a free-standing and binder-free electrode for next-generation LIBs.

In this work, we demonstrate a free-standing, binder-free graphene-silicon aerogel anode built up by freeze-drying. As shown in Scheme 1, commercial Si nanoparticles (100 mg) were first dispersed in aqueous solution of graphene oxide (GO) (17 mL, 3 mg mL^{-1}) by ultrasonication combined with mechanical stirring. The rich oxygen-contained functional groups and defect structure of GO sheets favors the anchoring of Si nanoparticles.[17,18] The ultrathin (0.8 nm), flexible, and wrinkly features of GO sheets are beneficial to wrap around Si. After freeze-drying in the home-made polytetrafluoroethylene mode, the GO-Si aqueous dispersion gave rise to the free-standing porous GO-encapsulated Si (Si@GO) aerogel. Followed by 1 h thermal treatment (1000 °C in Ar atmosphere with 3% H_2), graphene-encapsulated Si (Si@G) aerogel was obtained. The lightweight, flexible, and conductive graphene

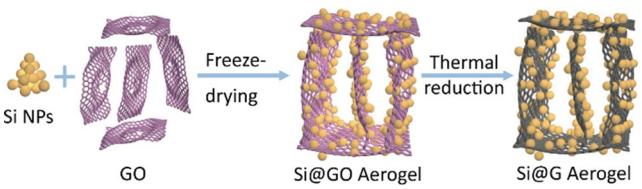

Scheme 1. Schematic of the Si@G aerogel fabrication process.

[a] Dr. X. Hu, Y. Jin, B. Zhu, Y. Tan, S. Zhang, L. Zong, Prof. Z. Lu, Prof. J. Zhu
National Laboratory of Solid State Microstructures
College of Engineering and Applied Sciences and Collaborative Innovation Center of Advanced Microstructures
Nanjing University
Nanjing (China)
E-mail: jiazhu@nju.edu.cn

Supporting information for this article can be found under http://dx.doi.org/10.1002/cnma.201600105.

This manuscript is part of a special issue on Nanomaterials for Energy Conversion and Storage. Click here to see the Table of Contents of the special issue.

framework not only plays a significant role in the electrical transport of Li^+, but also functions as a mechanical support and embedded-in current collector to ensure all Si nanoparticles keep good contact and are electrochemically active during the cycling. The free-standing Si@G aerogel showed excellent structural stability and good electrochemical performance, as shown below.

The inset in Figure 1a shows a typical photograph of three Si@G aerogel pieces 10 mm in diameter and 5 mm thick. The size of free-standing Si@G aerogel can be easily tuned by the modules used in freeze-drying. The obtained aerogel exhibited uniform porous structure with a pore size of 10–20 μm, as shown in Figure 1a, and the specific surface area was evaluated from N_2 adsorption–desorption isotherms to be 17.65 $m^2 g^{-1}$ (Figure S1). High-magnification scanning electron microscopy (SEM) showed Si nanoparticles anchored on both sides of graphene sheets homogeneously without apparent agglomeration (Figure 1b), and they were wrapped in the crumpled graphene sheets (Figure 1c).

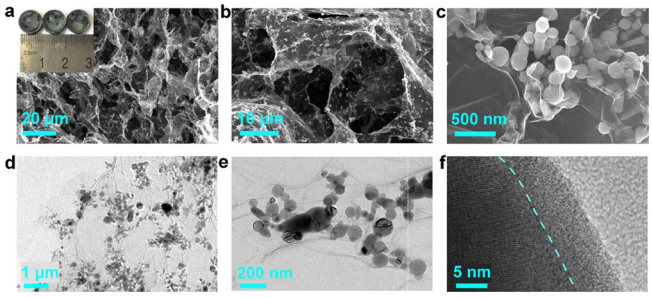

Figure 1. Morphology of the Si@G aerogel. (a–c) SEM images of the Si@G aerogel at different magnifications. Inset in (a) is a photograph of three Si@G aerogel pieces. (d–f) TEM images of Si@G aerogel at different magnification, showing Si nanoparticles are uniformly dispersed on the wrinkled graphene sheets.

We also used transmission electron microscopy (TEM) to characterize structures of Si@G aerogel (Figure 1d–f). In accordance with SEM images, both the wrinkled graphene sheets and Si nanoparticles were found, and Si nanoparticles were distributed on the graphene sheets evenly with little overlapped region. High resolution TEM images show there was a ≈7 nm SiO_x layer outside Si nanoparticles (Figure 1f). The oxidized coating layer could effectively prevent the formation of unstable SEI.[19]

X-ray diffraction (XRD) was used to examine the crystal structures as well as compositions of Si@GO and Si@G aerogel. As shown in Figure 2a, both XRD patterns show sharp peaks at 2 Theta of 29°, 47°, 56°, 69°, 77°, which are ascribed to crystalline Si nanoparticles.[20–22] After thermal reduction of Si@GO aerogel, the peak around 10° of GO disappears and the peak centered at 26° becomes much more obvious. The later corresponds to the diffraction from the (002) planes of graphite,[23] indicating a successful reduction of GO to graphene.

The surface chemical composition and functional groups were identified by X-ray photoelectron spectroscopy (XPS), as shown in Figure 2b. For Si@GO and Si@G aerogel, Si 2p

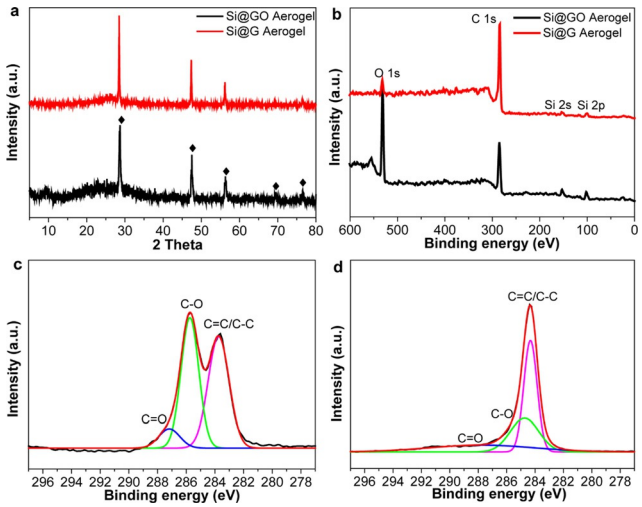

Figure 2. Composition of the aerogel. (a) XRD pattern of Si@GO aerogel and Si@G aerogel, the marked peaks belong to Si nanoparticles, (b) XPS spectra of Si@GO aerogel and Si@G aerogel, showing the decreased O content after reduction. High-resolution XPS spectra of C 1s and O 1s in the Si@GO aerogel (c) and Si@G aerogel (d).

(102 eV), Si 2s (153 eV), C 1s (285 eV), and O 1s (532 eV) signals were all detected in the XPS survey spectra. Compared with Si@GO aerogel, the intensity of O 1s peak decreases significantly while the C 1s peak strongly increases for Si@G aerogel. The deconvoluted C 1s spectra of Si@GO show three peaks at 283.7 eV, 285.7 eV, and 287.2 eV (Figure 2c), corresponding to C–C/C=C, C–O, and C=O, respectively.[24] After thermal reduction, these oxygen-containing groups decrease significantly, and the peak intensity corresponding to the sp^2 carbon increases and becomes narrower (Figure 2d), indicating the removal of oxygen-containing functional groups and the possible formation of C–C bonds during the reduction process. In addition, SEM and energy-dispersive X-ray spectroscopy (EDS) elemental mapping of Si@G aerogel also confirms the presence and uniform distribution of C and Si element (Figure S2), and Si nanoparticles are homogeneously combined with graphene.

The content of Si nanoparticles was determined by thermal gravimetric analysis (TGA) performed in N_2 atmosphere (Figure S3). GO aerogel loses about 43.5% weight around 200 °C due to the decomposition of the oxygen-containing functional groups. After the addition Si nanoparticles, the decomposition temperature increases to about 210 °C, indicating that Si nanoparticles could have interactions with the functional groups on GO sheets, which increases the energy barrier for releasing these groups. The weight loss of Si@GO aerogel is about 14.4 wt%, and the content of Si is calculated to be 66.8 wt% from the TGA curve, which is consistent with the feed ratio in raw materials. The content of Si nanoparticles in Si@G aerogel can also be calculated to be about 80 wt%.

The uniform porous structure and large Si content of the free-standing Si@G aerogel makes it very suitable for high performance LIB anodes. Figure 3 shows the electrochemical performance of Si@G aerogel. As shown in Figure 3a, the first charge and discharge capacity of Si@G aerogel anode were 2170 and 1499 mA h g^{-1} at a current density of 0.2 A g^{-1}, indi-

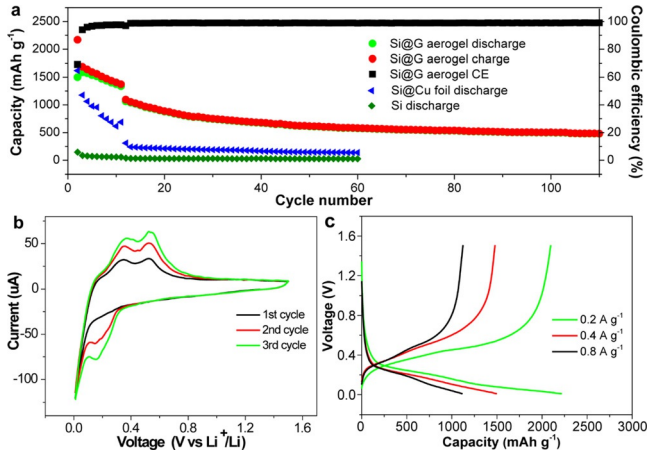

Figure 3. Electrochemical performance of Si@G aerogel. (a) Long-term cycling of Si@G aerogel anode, Si nanoparticles anode, and Si nanoparticle coating on Cu foil anode at a current density of 0.8 A g^{-1}. (b) Cyclic voltammetry curves of first three cycles of the Si@G aerogel in the potential window between 0.01 to 1.5 V at a rate of 0.1 mV s^{-1}. (c) Voltage profiles of Si@G aerogel at different current densities of 0.2, 0.4, and 0.8 A g^{-1}.

cating the initial coulombic efficiency (CE) of 69%. The loss of first reversible capacities can mainly be ascribed to the following two reasons: the irreversible reduction of the electrolyte to form a surface passivation layer on the Si nanoparticles, Li trapped in the porous structures of aerogel and defects on the reduced GO sheets. CE quickly increases to 94% in the second cycle, and then to above 99% after a few cycles.

For comparison, traditional electrodes on Cu foil were prepared by mixing Si nanoparticles, carbon black, and carboxymethylcellulose (CMC) binder (8:1:1, weight ratio) combined in DI water, followed by a blade-coating process (Sample A). Sample A shows quick capacity fading, from 1610 to 688 mA h g^{-1} within 10 cycles (57% decay), and limited cycle life. This is mainly because the ≈300% volume change of Si during lithiation and delithiation can lead to loss of electrical contact between Si and Cu foil, and CMC binder could block ion transport and degrade the electrical conductivity of anode. Si nanoparticle powder was also used as an anode (Sample B), and it shows very limited capacity (159 mA h g^{-1}), mainly ascribed to the poor electrical contact between adjacent Si nanoparticles. Our free-standing and binder-free Si@G aerogel demonstrates much improved electrochemical performance, which is expected as the graphene framework not only provides stable structures with good electrical network, but also wraps Si with large void space, allowing for volume expansion during electrochemical alloying. The discharge capacity of the first ten cycles only decreased slowly, from 1499 to 1377 mA h g^{-1} with 92% retained. Since the eleventh cycle, the current density was changed to 0.8 A g^{-1}, and the discharge capacity changes from 1062 mA h g^{-1} to 478 mA h g^{-1} after 100 cycles.

Cyclic voltammograms of the Si@G electrode in the first three cycles at a scanning rate of 0.1 mV s^{-1} between 0.01 and 1.5 V versus Li/Li^+ are shown in Figure 3b. The cathodic peak at around 0 V corresponds to the initial lithium insertion of crystalline Si, and crystalline Si transforms into amorphous Li_xSi. Because only crystalline Si exists at first, just one peak is observed during the lithiation process in the first cycle. In the delithiation procedure, the amorphous Li_xSi converts to amorphous Si, thus two typical redox peaks at 0.35 V and 0.53 V appear, and in the subsequent cathodic scans, a new characteristic peak of amorphous Si presents at 0.16 V. Figure 3c shows the typical discharge–charge profiles of Si@G aerogel between 0.01 and 1.5 V at different current densities of 0.2 A g^{-1}, 0.4 A g^{-1}, 0.8 A g^{-1}.

The morphology of Si@G anode after 100 lithiation–delithiation cycles at 0.8 A g^{-1} was investigated to prove the structure stability. As shown in Figure 4, the porous structure of Si@G aerogel remains almost the same as the initial state, and Si nanoparticles are still anchored on the graphene sheets evenly and remain in good contact.

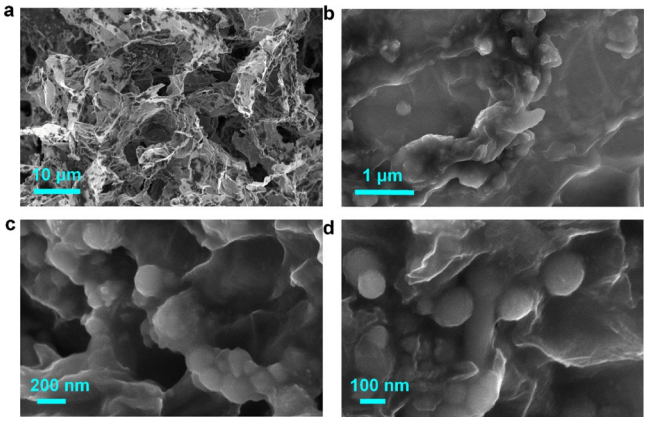

Figure 4. SEM images of Si@G aerogel after 100 charge–discharge cycles at a current density of 0.8 A g^{-1}. Si nanoparticles are still anchored on graphene sheets.

In summary, free-standing and binder-free Si@G aerogel was fabricated by a facile freeze-drying strategy. This free-standing aerogel successfully integrated Si nanoparticles into the lightweight, flexible, and conductive graphene framework. Graphene nanosheets functioned as a mechanical skeleton, which provided anchoring sites to Si, and were also a lightweight current collector embedded in the active materials on the nanoscale. The porous structure was very stable and Si nanoparticles were found anchored on the graphene sheets uniformly even after 100 charge–discharge cycles, providing the obtained Si@G aerogel good electrochemical performance. After 50 charge–discharge cycles at a current density of 0.8 A g^{-1}, the specific capacity remains at 617 mA h g^{-1}, 18 times that of the Si nanoparticle powder anode, and 4 times that of traditional Si electrode on Cu foil by typical slurry method. Compared with previous studies, the weight of the electrode was significantly decreased by replacing the heavy metal foils. Our free-standing Si@G aerogel paves the way for LIBs with higher energy density and power density.

Experimental Section

Material characterization

The morphologies and structures of the as-prepared aerogel were characterized by scanning electron microscopy (Dual-beam FIB 235, FEI Strata) and transmission electron microscopy (JEM-200CX). XRD spectra was obtained on a Rigaku Ultima X-ray IV diffractometer using a $Cu_{K\alpha}$ at $5^{\circ}\,min^{-1}$. XPS spectra were obtained on THERMO FISHERSCIENTIFIC K-Alpha. The weight percentage of Si and C in the aerogel was determined from the weight loss curves measured under N_2 atmosphere on a TG instrument (Netzsch STA 409PC) with a heating rate of $10\,^{\circ}C\,min^{-1}$.

Electrochemical testing

The electrochemical properties were evaluated by galvanostatic cycling of coin cells with lithium foil as the counter/reference electrode. Free-standing Si@G aerogel, traditional Si@Cu foil electrode, and Si powder were all utilized as the working electrode. Si@Cu foil electrodes were prepared by mixing Si nanoparticles, carbon black, and CMC binder (8:1:1, weight ratio) combined in DI water, followed by blade-coating process. Si nanoparticle powder was directly used as anode. Coin-type cells (2032) were fabricated inside an Ar-filled glove box using a celgard 2250 separator. The electrolyte employed was 1.0 M $LiPF_6$ in 1:1 vol/vol ethylene carbonate/diethyl carbonate with 2 mole% vinylene carbonate (Guotai Huarong Corporation) added to improve the cycling stability. The mass loadings of Si@G aerogel, Si@Cu foil, and Si powder anodes were 1.2, 0.32, 0.2 $mg\,cm^{-2}$, respectively. Galvanostatic cycling was performed using a LANHE CT2001 A, the galvanostatic voltage cutoffs were 0.01 and 1.5 V vs Li/Li^+. The specific capacity was calculated based on the mass of Si. Cyclic voltammograms were measured on a CHI660E workstation (CH Instruments, Shanghai) in the voltage range of 1.5–0.01 V under a scanning rate of $0.1\,mV\,s^{-1}$.

Acknowledgements

This work is jointly supported by the State Key Program for Basic Research of China (No. 2015CB659300), National Natural Science Foundation of China (NSFC No. 11321063 and No. 11574143), Natural Science Foundation of Jiangsu Province (No. BK20150056), the Priority Academic Program Development of Jiangsu Higher Education Institutions (PAPD) and the Fundamental Research Funds for the Central Universities.

Keywords: aerogel · free-standing · graphene · lithium ion battery · silicon

[1] M. Armand, J. M. Tarascon, *Nature* **2008**, *451*, 652–657.
[2] H. Wu, Y. Cui, *Nano Today* **2012**, *7*, 414–429.
[3] N. S. Choi, Y. Yao, Y. Cui, J. Cho, *J. Mater. Chem.* **2011**, *21*, 9825–9840.
[4] A. S. Aricò, P. Bruce, B. Scrosati, J. M. Tarascon, W. VanSchalkwijk, *Nat. Mater.* **2005**, *4*, 366–377.
[5] X. Su, Q. L. Wu, J. C. Li, X. C. Xiao, A. Lott, W. Q. Lu, B. W. Sheldon, J. Wu, *Adv. Energy Mater.* **2014**, *4*, 1300882.
[6] C. K. Chan, H. L. Peng, G. Liu, K. McIlwrath, X. F. Zhang, R. A. Huggins, Y. Cui, *Nat. Nanotechnol.* **2008**, *3*, 31–35.
[7] M. H. Park, M. G. Kim, J. Joo, K. Kim, J. Kim, S. Ahn, Y. Cui, J. Cho, *Nano Lett.* **2009**, *9*, 3844–3847.
[8] Z. D. Lu, N. Liu, H. W. Lee, J. Zhao, W. Y. Li, Y. Z. Li, Y. Cui, *ACS Nano* **2015**, *9*, 2540–2547.
[9] Y. Jin, S. Zhang, B. Zhu, Y. L. Tan, X. Z. Hu, L. Q. Zong, J. Zhu, *Nano Lett.* **2015**, *15*, 7742–7747.
[10] Y. Yao, M. T. McDowell, I. Ryu, H. Wu, N. A. Liu, L. B. Hu, W. D. Nix, Y. Cui, *Nano Lett.* **2011**, *11*, 2949–2954.
[11] M. Y. Ge, J. P. Rong, X. Fang, C. W. Zhou, *Nano Lett.* **2012**, *12*, 2318–2323.
[12] A. Magasinski, P. Dixon, B. Hertzberg, A. Kvit, J. Ayala, G. Yushin, *Nat. Mater.* **2010**, *9*, 353–358.
[13] H. Wu, G. Chan, J. W. Choi, I. Ryu, Y. Yao, M. T. McDowell, S. W. Lee, A. Jackson, Y. Yang, L. B. Hu, Y. Cui, *Nat. Nanotechnol.* **2012**, *7*, 309–314.
[14] N. Liu, H. Wu, M. T. McDowell, Y. Yao, C. M. Wang, Y. Cui, *Nano Lett.* **2012**, *12*, 3315–3321.
[15] N. Liu, Z. D. Lu, J. Zhao, M. T. McDowell, H. W. Lee, W. T. Zhao, Y. Cui, *Nat. Nanotechnol.* **2014**, *9*, 187–192.
[16] Z. Cao, B. Wei, *J. Power Sources* **2013**, *241*, 330–340.
[17] D. R. Dreyer, S. Park, C. W. Bielawski, R. S. Ruoff, *Chem. Soc. Rev.* **2010**, *39*, 228–240.
[18] Z. Wang, Y. Dong, H. Li, Z. Zhao, H. B. Wu, C. Hao, S. Liu, J. Qiu, X. W. Lou, *Nat. Commun.* **2014**, *5*, 1–8.
[19] X. Xin, X. Zhou, F. Wang, X. Yao, X. Xu, Y. Zhu, Z. Liu, *J. Mater. Chem.* **2012**, *22*, 7724–7730.
[20] B. Zhu, Y. Jin, Y. L. Tan, L. Q. Zong, Y. Hu, L. Chen, Y. B. Chen, Q. Zhang, J. Zhu, *Nano lett.* **2015**, *15*, 5750–5754.
[21] B. H. Xu, H. Wu, C. X. Lin, B. Wang, Z. Zhang, X. S. Zhao, *RSC Adv.* **2015**, *5*, 30624–30630.
[22] V. Chabot, K. Feng, H. W. Park, F. M. Hassan, A. R. Elsayed, A. P. Yu, X. C. Xiao, Z. W. Chen, *Electrochim. Acta* **2014**, *130*, 127–134.
[23] Y. Xu, H. Bai, G. Lu, C. Li, G. Shi, *J. Am. Chem. Soc.* **2008**, *130*, 5856–5857.
[24] S. Stankovich, D. A. Dikin, R. D. Piner, K. A. Kohlhaas, A. Kleinhammes, Y. Y. Jia, Y. Wu, S. T. Nguyen, R. S. Ruoff, *Carbon* **2007**, *45*, 1558–1565.

Manuscript received: March 15, 2016
Revised: April 8, 2016
Final Article published: May 24, 2016